Performance and Reliability of Solid Tantalum Capacitors at Cryogenic Conditions

Alexander Teverovsky

QSS Group, Inc.
Code 562, NASA GSFC, Greenbelt, MD 20771
Alexander.A.Teverovsky.1@gsfc.nasa.gov

Abstract

Performance of different types of solid tantalum capacitors was evaluated at room and low temperatures, down to 15 K. The effect of temperature on frequency dependencies of capacitance, effective series resistances (ESR), leakage currents, and breakdown voltages has been investigated and analyzed. To assess thermo-mechanical robustness of the parts, several groups of loose capacitors and those soldered on FR4 boards were subjected to multiple (up to 500) temperature cycles between room temperature and 77 K.

Experiments and mathematical modeling have shown that degradation in tantalum capacitors at low temperatures is mostly due to increasing resistance of the manganese cathode layer, resulting in substantial decrease of the roll-off frequency. Absorption currents follow a power law, $I \sim t^{-m}$, with the exponent m varying from 0.8 to 1.1. These currents do not change significantly at cryogenic conditions and the value of the exponent remains the same down to 15 K. Variations of leakage currents with voltage can be described by Pool-Frenkel and Schottky mechanisms of conductivity, with the Schottky mechanism prevailing at cryogenic conditions. Breakdown voltages of tantalum capacitors increase and the probability of scintillations decreases at cryogenic temperatures. However, breakdown voltages measured during surge current testing decrease at liquid nitrogen (LN) compared to room-temperature conditions. Results of temperature cycling suggest that tantalum capacitors are capable of withstanding multiple exposures to cryogenic conditions, but the probability of failures varies for different part types.

Introduction

Space exploration programs often require that sensors and instruments with related service electronics are exposed to outer space, thus subjecting them to extreme environmental conditions. In programs such as Lunar and Martian expeditions and deep-space exploration, these conditions include cryogenic temperatures.

Tantalum and/or ceramic capacitors are widely used at the power supply pins of microcircuits to short high-frequency signals and provide the necessary charge during burst increases of the load currents. The decoupling capacitors should have minimal effective series resistance (ESR) and a value that is about 10 times greater than the sum of the switched capacitors so that the power supply voltage would not change significantly during discharging. Typically, most capacitors decrease their values as the temperature decreases [1-3]. However, there is no sufficient information in literature regarding frequency dependencies of C and ESR at cryogenic temperatures, and the mechanism of parametric degradation of tantalum capacitors at these conditions has not been investigated properly yet.

A failure of a tantalum capacitor used in power supply lines would cause a short circuit and result in a catastrophic failure in the system. Typically, a current surge test is performed to assure the robustness of the parts to transient currents, but no such data have been available yet for cryogenic conditions.

During the ground phase integration and testing period of a space system, the parts are subjected to multiple exposures to cryogenic conditions. This requires investigation of the effect of multiple cryo-cycling on the behavior of parts intended for cryogenic applications.

In this work, performance of different types of solid tantalum capacitors was evaluated at room and low temperatures, down to 15 K. The effect of temperature on frequency dependencies of capacitance, and values of ESR, leakage currents, and breakdown voltages have been investigated and analyzed. To assess thermo-mechanical robustness of the parts, several groups of capacitors were subjected to multiple (up to 500) temperature cycles between room temperature and 77 K. Mechanisms of degradation of AC and DC characteristics at cryogenic conditions are discussed.

Experiment

Frequency characteristics of capacitors were measured using an HP4192A LF impedance analyzer. Polarization and depolarization currents (currents in a biased and in a short-circuited capacitor) were measured with time at different voltages and temperatures using a precision semiconductor analyzer HP4156A. Step stress surge current testing (SSST) was carried out using a PC-based system with the effective resistance of the circuit ~0.3 Ohm.

Experiments were carried out on different types of commercial leaded and chip solid tantalum capacitors manufactured by Kemet and AVX with manganese cathodes (see Table 1). Three samples minimum of each type were used for testing.

Table 1. Capacitors used for testing.

PN	C, uF	V, V
TAP106K050SCS	10	50
TAP106K025SCS	10	25
T495X156M050AS	15	50
T491A155K016AS	1.5	16
T491C106K016AS	10	16
T491D226M035AS	22	35

Low-temperature measurements were carried out either at a liquid nitrogen temperature (LN conditions, T = 77 K) or in a Cryodyne chamber allowing testing down to 15 K.

For cryo-cycling, different groups of capacitors were placed in hermetic cells and immersed periodically into LN dewar using a PC-based system, which controlled a mechanical armature and allowed monitoring of the temperature inside the cells. The dwell time at temperature extremes was ~3 min., and a maximum temperature rate was ~40 °C/min. for loose parts and ~20 °C/min. for parts soldered on FR4 boards.

Frequency Dependencies of C and ESR

Figure 1 shows typical frequency dependencies of capacitance for two part types at room and cryogenic temperatures. At low frequencies (<0.1 kHz), a decrease of C is relatively small (10% to 30%), whereas at high frequencies capacitance decreases five to seven times. This behavior is due to the so-called roll-off effect, in which a slope of C-f characteristics of tantalum capacitors increases when frequency exceeds the roll-off frequency, f_r. The effect is qualitatively explained by an R-C-ladder behavior of the capacitor in the frequency domain [4].

A characteristic feature of the C-f dependencies measured at low temperatures is a significant decrease of f_r with temperature. At room temperature f_r is ~10 to 30 kHz and decreases to ~1 kHz at LN conditions and to ~0.1 kHz at 15 K.

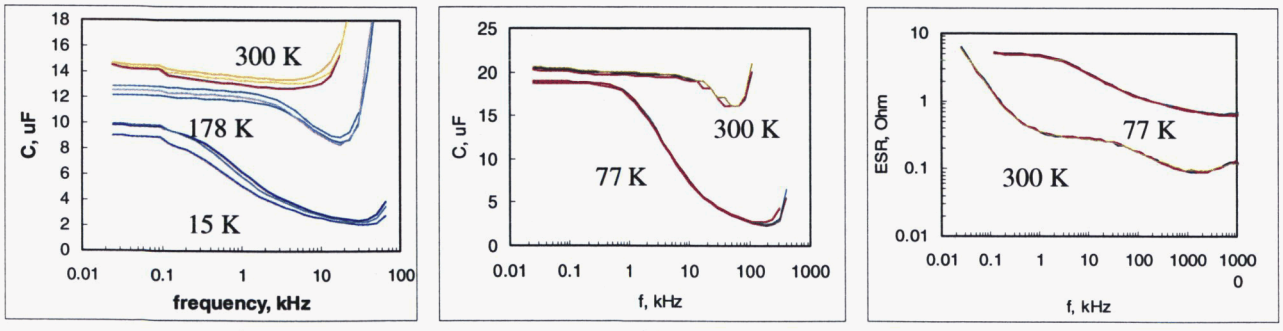

a) b) c)

Figure 1. Frequency dependence of capacitance (a, b) and ESR (c) at different temperatures for three 15 μF/50 V (a) and three 22 μF/35 V (c) capacitors.

Average values of capacitance measured at 1 kHz and ESR measured at 100 kHz for different part types are summarized in Table 2. At 1 kHz a decrease of C at 77 K is relatively small and varies from 7% to 26%, whereas ESR increases more dramatically, from four to 18 times. This increase of ESR is most likely due to temperature variations of the resistivity of manganese cathode layers.

Table 2. Average values of capacitance and ESR at room and liquid nitrogen temperatures.

Type	C, μF		ESR, Ohm	
	RT	LN	RT	LN
10 uF 50 V	10.3	8.8	0.42	2.4
10 uF 25 V	9.6	8.9	0.36	2.2
15 uF 50 V	15.1	11.1	0.19	0.73
10 uF 16 V	10.1	8.6	0.45	7.9
1.5 uF 16 V	1.5	1.35	4.8	89
22 uF 35 V	19.8	17.3	0.17	1.1

To explain the observed frequency variations at low temperatures, a tantalum capacitor was represented with a distributed one-dimensional R-G-C circuit shown in Figure 2. In this figure ρ is the specific (per unit length) surface resistivity of the manganese layer, and C_o and g are the specific capacitance and conductance of the tantalum pentoxide layer.

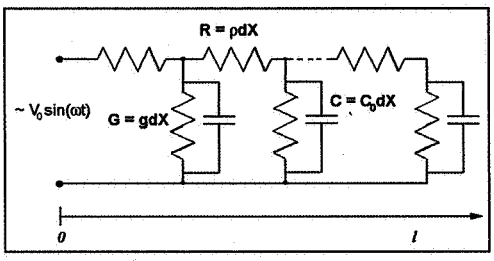

Figure 2. Equivalent schematic of a tantalum capacitor.

Distribution of the potential, $V(x,t)$, along this R-G-C ladder is given by equation:

$$\frac{\partial u}{\partial \theta} = \frac{\partial^2 u}{\partial \xi^2} - \alpha \times u^2, \tag{1}$$

where $u = V/V_o$, $\xi = x/l$, $\theta = t/(C_o \times \rho \times l^2)$, $\alpha^2 = g \times \rho \times l^2$.

Assuming that an AC signal applied to the capacitor has a circular frequency ω, the border conditions can be written as follows:

$$\left.\begin{aligned} u(0,\theta) &= \sin(\omega' \times \theta) \\ \frac{\partial u}{\partial \xi}(1,\theta) &= 0 \\ u(\xi,0) &= 0 \end{aligned}\right\}, \tag{2}$$

where $\omega' = \omega \times \rho \times C_o \times l^2$.

Input currents at the beginning of the ladder can be expressed through the voltage gradient:

$$I_0 = V_0 \times \left.\frac{\partial u}{\partial \xi}\right|_{\xi=0} \times \frac{1}{\rho \times l}$$

This allows calculation of the equivalent capacitance of the ladder:

$$C_{eq} = \frac{I_0}{\omega \times V_0}$$

Using a solution for the problem Eq. (1, 2) at stationary-state conditions [5] and neglecting g, the expression for C_{eq} can be written as:

$$C_{eq} = 2 \times l \times \sqrt{A^2 + B^2}\ , \qquad (3)$$

where

$$A = \sum_1^{\infty} \frac{C_0 \times \omega'}{\lambda_n^4 + \omega'^2}.,...B = \sum_1^{\infty} \frac{C_0 \times \lambda_n^2}{\lambda_n^4 + \omega'^2}.,...\lambda_n = \frac{(2n-1) \times \pi}{2}.,\ \ n = 1, 2, 3, \ldots$$

An effective length and surface area of electrodes of a typical chip tantalum capacitor are l ~3 mm and S ~100 cm^2, and the thickness of Ta_2O_5 dielectric, h, ~3×10^{-4} cm [6]. At room temperature, the values of the specific volume resistivity, ρ_v, of MnO_2 vary from 1 Ohm*cm to 10 Ohm*cm [4, 7, 8]. At these conditions the equivalent specific resistivity, which is $\rho = \rho_v l/(Sh)$, will be ~10 to 100 Ohm/cm. Based on the ESR measurements, the resistance of MnO_2 is increasing at liquid nitrogen conditions in four to 18 times resulting in variation of ρ from 40 to 1,800 Ohm/cm. These relatively weak temperature variations are in agreement with an assumption that manganese dioxide is a N-type semiconductor with a shallow donor level having energy of ~40 meV [9].

Using these data, frequency dependencies of capacitance were calculated for a 10 μF capacitor at the effective surface resistances of MnO_2 layer ranging from 10 to 1,800 Ohm/cm. Results of these calculations are displayed in Figure 3. A comparison with Figure 1 shows reasonably good agreement with the experimental data. Assuming that the value of ρ of MnO_2 at RT is ~10 Ohm/cm, the calculated roll-off frequency, f_r, is ~10 kHz. An increase of ρ_v to 300 Ohm/cm at LN conditions decreases f_r to ~1 kHz, which corresponds to the experimental data.

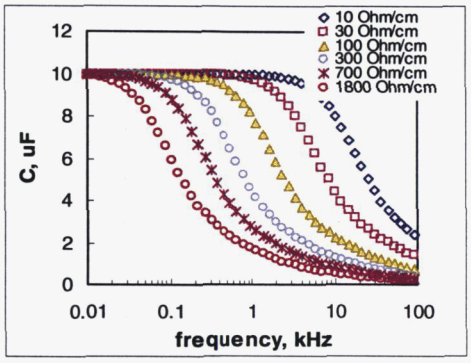

Figure 3. Frequency dependencies of a 10 μF tantalum capacitor at different surface resistivity of manganese cathodes calculated according to Eq. (3).

The results indicate that at low temperatures and relatively high frequencies, $f > f_r$, a significant decrease in C is due to increase of the resistance of manganese cathode. Contrary to that, at low frequencies, $f < f_r$, a relatively small decrease of capacitance is due to temperature variations of the dielectric constant of tantalum pentoxide dielectric. It is worth noting that tantalum capacitors with polymer cathodes, which remain at high conductivity at low temperatures, do not degrade significantly at cryogenic conditions [10].

Leakage Currents

A forward current (normal polarity) in a tantalum capacitor is a sum of time-dependent absorption currents and time-independent leakage currents [6]. Absorption currents are due to accumulation of trapped charges in Ta_2O_5 dielectric and decrease with time after applying voltage following a power law, I ~t^{-m}, with the exponent m varying at room temperature from 0.8 to 1.1.

Figure 4 shows typical time dependence of forward currents (I-t characteristics) for a 15 μF 50 V capacitor at different temperatures. It is seen that at the rated voltage, after 5 min. leakage currents can be observed at room temperature only, and at low temperatures they decrease below the nanoampere range. This agrees with the reported activation energies of leakage currents, which vary from 0.3 to 0.7 eV [6, 11]. Even at Ea = 0.3 eV, the leakage currents would decrease more than 10^{15} times as the temperature decreases from room to LN conditions.

Absorption currents follow a power law, $I \sim t^{-m}$, down to 15 K and do not change with temperature significantly, decreasing about three times only between RT and LN conditions and about five times down to 15 K. The exponent m does not depend on temperature significantly, remaining in the range from 0.9 to 1.1. Depolarization currents also decrease with time according to a power law with the exponent close to the one for polarization currents.

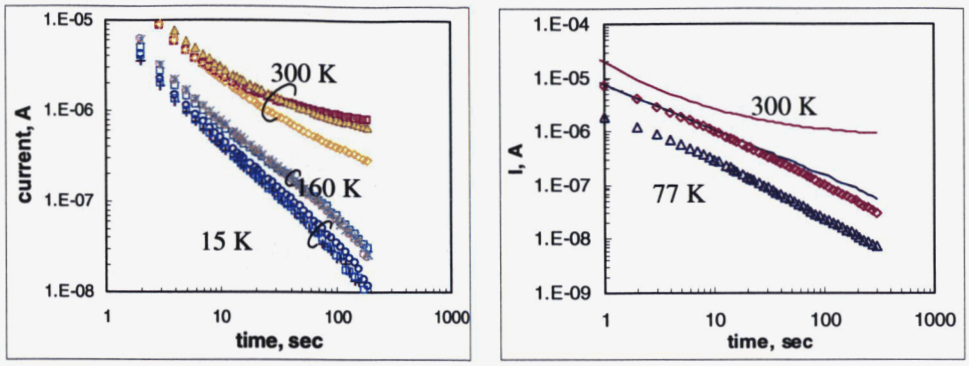

a) b)

Figure 4. Relaxation of currents in 15 μF/50 V capacitors at different temperatures. Polarization currents, m ~1.1 (a); polarization (lines) and depolarization (marks) currents, m ~1.

Voltage dependence of leakage currents in Ta_2O_5 is explained usually either by a bulk-limited Pool-Frenkel (PF) mechanism of conductivity or by a surface-barrier-limited Schottky mechanism [12-14]. The PF mechanism can be described by the following equation:

$$J = C_t E \exp\left(-\frac{q\Phi}{kT}\right)\exp\left(-\frac{\beta_{PF}E^{1/2}}{kT}\right), \quad (4)$$

where J is the current density, C_t is a trap density related constant, E is the electric field, q is the charge of electron, Φ is the barrier height, k is the Boltzmann constant, and T is the absolute temperature; and

$$\beta_{PF} = \left(\frac{q^3}{\pi\varepsilon_0\varepsilon}\right)^{1/2}$$

is the PF constant, ε_0 is the permittivity of the free space, and ε is the high-frequency dielectric constant, which for Ta_2O_5 is $\varepsilon_{HF} \approx 5$.

A corresponding equation for the Schottky mechanism can be written as:

$$J = C_{RD}T^2 \exp\left(-\frac{q\Phi}{kT}\right)\exp\left(\frac{\beta_S E^{1/2}}{kT}\right), \quad (5)$$

where $\beta_S = \left(\frac{q^3}{4\pi\varepsilon_0\varepsilon}\right)^{1/2}$ and C_{RD} is the Richardson-Dushman constant.

To discriminate between these two mechanisms, the dielectric constant ε was calculated based on experimentally determined values of slopes β_{PF} and β_S. The values of leakage currents (in our experiments, the currents were measured in 5 min. after voltage application) in different groups of capacitors were measured at room and LN conditions at voltages varying from the rated to the breakdown voltage in 5 V increments. The data were plotted in PF coordinates, $ln(I/E)$ vs $E^{0.5}$, and in Schottky coordinates, $ln(I)$ vs. $E^{0.5}$. The electric field E was calculated as $E = V/h$, where the thickness h was assumed to be 110 nm, 240 nm, and 350 nm for 16 V, 35 V, and 50 V capacitors, respectively. Figure 5 shows results of these experiments for 10 μF/16 V capacitors. Similar charts were obtained for other part types.

At room temperature, deviations from the straight line are due most likely to a significant contribution of the absorption currents, which do not follow PF or Schottky mechanisms. In all cases, at relatively large $E > 3*10^6$ V/cm I-V characteristics could be could be equally well approximated with both equations having R-squared values for the regression trendlines exceeding 0.995.

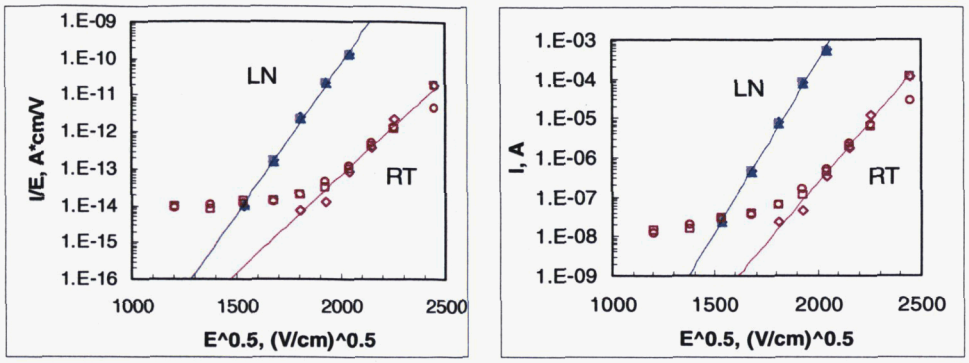

a) b)

Figure 5. I-V characteristics of 10 μF 16 V Ta capacitors at RT and LN conditions in Pool-Frenkel (a) and Schottky (b) coordinates.

In an attempt to discriminate between these models, the values of high-frequency dielectric constants were calculated for the PF, ε_{PF}, and Schottky, ε_S, models (see Table 3). At room temperature, ε_S varies from 0.5 to 4, whereas ε_{PF} varies from 2.4 to 11.6. These data suggest that at room temperature the PF conductivity is more probable compared to the Schottky-controlled mechanism. At LN conditions the situation is different, and the values of ε_{PF} (from 32.6 to 93.7) are much higher than the expected value of the high-frequency dielectric constant. The values of ε_S at cryogenic condition values vary in a relatively narrow range, from 8.2 to 8.7, which is reasonably close to ε_{HF}.

Table 3. Calculated values of the dielectric constant.

Part	PF RT	Sch RT	PF LN	Sch LN
1.5 uF 16 V	11.6	2.33	39	8.24
10 uF 16 V	5.8	1.08	36.9	8.25
22 uF 35 V	10.6	4.03	32.6	7.26
15 uF 50 V	2.4	0.53	93.7	8.67

It should be noted that in the presence of multi-level traps and partial compensation of the donor centers, the number of electrons participating in conduction decreases and the conduction can be described by a modified PF equation [12, 13, 15]:

$$J = C_t E \exp\left(-\frac{q\Phi}{kT}\right)\exp\left(-\frac{\beta_{PF}E^{1/2}}{rkT}\right),$$

where r is a coefficient in the modified PF effect with compensation.

Use of the modified Poole-Frenkel model can decrease the estimated values of ε probably up to four times; however, even in this case, they remain larger than those obtained by the Schottky model. This indicates that at cryogenic temperatures, the mechanism of conduction in tantalum capacitors most likely changes from the bulk-controlled PF trap-assisted conductivity to a surface-barrier-controlled Schottky mechanism.

Breakdown Voltages

As the voltage applied to a tantalum capacitor increases a so-called scintillation current, spikes appear in the I-t curve as can be seen in Figure 6. These momentary current pulses are believed to be due to a local breakdown of the Ta_2O_5 dielectric, which is terminated by a self-healing mechanism [16]. According to this mechanism, temperature of the manganese cathode in areas of breakdown increases, resulting in conversion of conductive MnO_2 into a high-resistive Mn_2O_3 (~10^4 ohm*cm) and thus effectively reducing breakdown currents. Comparison of typical results of I-t measurements at RT and LN conditions shown in Figure 6 suggests that at 77 K scintillations are observed at much higher voltages than at room temperature.

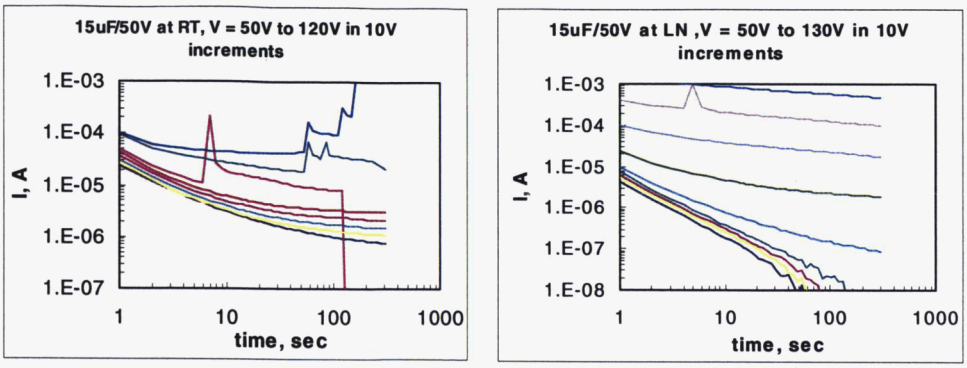

a) b)

Figure 6. Typical I - t characteristics of 15 μF/50 V capacitors during step voltage testing at room (a) and liquid nitrogen (b) conditions.

To assess the effect of temperature on breakdown voltages quantitatively, two groups of 15 μF 50 V capacitors with nine samples in each group were tested for 5 min. at voltages increasing with 10 V increments. The scintillation breakdown voltage, V_S, was determined as the voltage at which the first current spike is observed.

Results of these experiments are presented in Weibull coordinates in Figure 7a. At room-temperature conditions, the characteristic scintillation voltage was ~40% lower than at LN conditions (148.7 V and 105.3 V, respectively). The slope of the distributions was similar and varied in the range from β = 7.8 to 8.8, suggesting that at both temperatures the mechanism of breakdown was similar. These results are consistent with the overall trend of increasing breakdown voltages of dielectrics at cryogenic conditions [17].

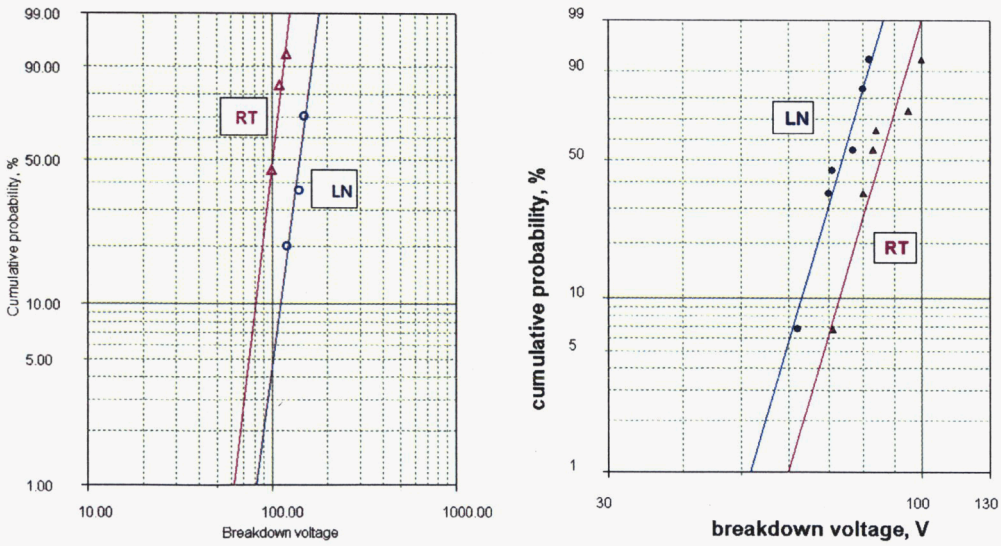

a) b)

Figure 7. Weibull distributions of breakdown voltages for 15 μF/50 V capacitors: a) scintillation breakdown voltages, and b) step surge current test breakdown voltages.

Distributions of the breakdown voltages measured during step surge stress testing (SSST) at room-temperature and liquid nitrogen conditions are shown in Figure 7b. Similar to scintillation measurements, both distributions were parallel with the slope β varying from 11 to 12, but the characteristic breakdown voltage, V_{SSST}, at LN (75.9 V) was ~ 40% lower that at room temperature (88.1 V).

The difference in the effect of temperature on breakdown voltages measured during scintillation testing and surge current testing is due to different mechanisms of breakdown in high- and low-impedance circuits. Although the mechanism of failures under surge current testing and factors affecting the probability of failures are not well understood yet, it is known that there is no correlation between the breakdown voltage and leakage currents in tantalum

capacitors [18]. Our data indicate also that V_{SSST} is not related directly to the breakdown voltage of the tantalum pentoxide dielectric.

Effect of Cryo-cycling

Two lots of 15 μF/50 V capacitors with different date codes and one lot of 22 μF/35 V capacitors were subjected to temperature cycling between room-temperature and LN conditions. Each batch had 10 to 15 parts. Characteristics of the parts were measured periodically during this testing, which continued until 500 cycles were completed for loose parts and 100 cycles were completed for the parts soldered on FR4 boards.

All observed failures were due to increased leakage currents, whereas capacitance and ESR did not change substantially. Figure 8 shows variations of leakage currents through the testing for loose parts. In the first lot of 15 μF capacitors, 80% of the parts failed by the end of testing, whereas only one out of 10 parts failed in the 22 μF batch, and the second lot of 15 μF capacitors had no failures. No failures were observed also after 100 cycles of parts soldered onto the boards.

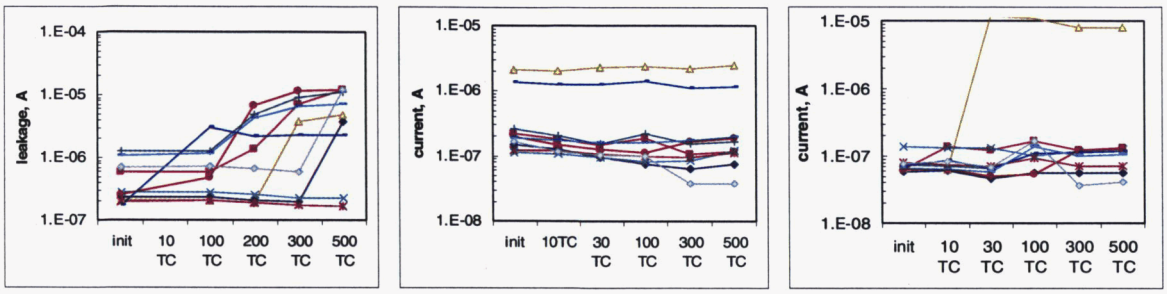

a) b) c)

Figure 8. Variations of leakage currents during temperature cycling between RT and LN temperatures for 15 μF/50 V lot I (a), 15 μF/50 V lot II (b), and 22 μF/35 V capacitors.

The results indicate that different lots of tantalum capacitors might have different susceptibilities to multiple exposures to low temperatures, and cryo-cycling should be used to qualify each perspective lot for cryogenic applications. Temperature cycling of the parts soldered on the boards was expected to cause more failures compared to loose parts due to development of additional mechanical stresses caused by CTE mismatch between the part and the board materials. However, experiments did not reveal failures in soldered parts up to 100 cycles. It is possible that this is due to a lesser rate of temperature variations during cycling of the boards. Additional experiments are necessary to evaluate the effect of soldering on results of temperature cycling.

Conclusions

- At relatively low frequencies, $f < f_r$, solid tantalum capacitors decrease their value at LN compared to RT conditions on less that ~30%. However, at $f > f_r$ the decrease of C might be as large as five to seven times. The ESR values measured at 100 kHz increase four to 18 times at 77 K compared to RT conditions.
- Simulation of a tantalum capacitor with a one-dimensional RC ladder have shown that variations of frequency dependence and decrease of capacitance at low temperatures is mostly due to an increase of resistance of the manganese cathode layer, resulting in substantial decrease of the roll-off frequency.
- Absorption currents, which prevail in tantalum capacitors during the first several minutes after applying the voltage, do not change significantly at low temperatures down to 15 K and follow a power law, $I \sim t^{-m}$, with the exponent m varying from 0.8 to 1.1.
- Leakage currents increase exponentially with voltage and can be explained by a surface-barrier-limited Schottky mechanism or bulk-limited Pool-Frenkel mechanism of conductivity. Based on ε_{HF} estimations, Schottky conduction prevails at cryogenic conditions, whereas the Pool-Frenkel mechanism gives more adequate results at room temperature.
- Breakdown voltages of tantalum capacitors, measured at the first scintillation, increase ~40% at LN compared to RT conditions. However, breakdown voltages measured during step surge current testing decrease ~40% at 77 K. This indicates that reliability of tantalum capacitors at cryogenic conditions might increase for high-impedance applications and decreases for low-impedance applications.
- Results of temperature cycling suggest that tantalum capacitors are capable of withstanding 500 cycles between 300 K and 77 K, but the probability of failures varies for different part types. Reliability qualification testing of

tantalum capacitors should include cryo-cycling and should be performed on each lot of parts intended for cryogenic applications.

Acknowledgments

This work was sponsored by the Goddard Space Flight Center Projects and NASA Electronic Parts and Packaging (NEPP) Program. The author is thankful to Darryl Lakins, the Head of Code 562; Michael Sampson, the NEPP Program Manager, who recognized the need for this investigation; and to Jeanne Ilg and Hang Ngin for technical support and assistance with testing.

References

1. R. L. Patterson, A. Hammoud, J. E. Dickman, S. Gerber, M. E. Elbuluk, and E. Overton, "Electrical devices and circuits for low temperature space applications," in Proceedings of the International Workshop on Thermal Detectors (TDW03), June 19-20, 2003, Washington, DC.
2. A. Hammoud, S. Gerber, R. L. Patterson, and T. L. MacDonald, "Performance of surface-mount ceramic and solid tantalum capacitors for cryogenic applications," in Proceedings of the Conference on Electrical Insulation and Dielectric Phenomena, Annual Report, Oct. 25-28, 1998, pp. 572-576.
3. J. Gornto, T. Green, W. Symon, and R. W. Johnson, "Passive components for Lunar and Martian exploration," in Proceedings of the Reliability of Advanced Electronic Packages and Devices in Extreme Cold Environments, February 21-23, 2005, Pasadena, CA.
4. J. D. Prymak, "New tantalum capacitors in power supply applications," in Proceedings of the 1998 IEEE Industry Applications Conference, Thirty-Third IAS Annual Meeting, Oct. 12-15, 1998, pp. 1129-1137.
5. A. N. Tikhonov and A. A. Samarskii, Equations of Mathematical Physics, 1990, Dover Books on Physics and Chemistry, p. 754.
6. A. Teverovsky, "Reverse bias behavior of surface mount tantalum capacitors," in Proceedings of the CARTS 2002, pp. 105-123.
7. J. Gill, "Basic tantalum capacitor technology," AVX Technical Information, 1994.
8. R. Hahn and K. Pritchard, "Strategies for manufacturing ultra low ESR Ta capacitors," in Proceedings of the 25th CARTS USA 2005, March 21-24, 2005, Palm Springs, CA, pp. 225-231.
9. J. S. J. Pavelka, P. Vasina, V. Sedlakova, M. Tacano, and S. Hashiguchi, "Noise and transport characterisation of tantalum capacitors," in Microelectronics Reliability, 2002, 42, pp. 841-847.
10. A. Teverovsky, "Performance of decoupling capacitors at cryogenic conditions," in Proceedings of the 10th Annual International Conference, Components for Military and Space Electronics, CMSE'06, February 6-9, 2006, Los Angeles, CA, pp. 456-466.
11. R. S. K. H. Allers, W. Walter, M. Schrenk, and H. Korner, "Thermal and dielectric breakdown for metal insulator metal capacitors (MIMCAP) with tantalum pentoxide dielectric," in Proceedings of the IEEE International Integrated Reliability Workshop Final Report, Oct. 21-24, 2002, pp. 96-101.
12. J. L. A. C. Chaneliere, R. A. B. Devine, and B. Balland, "Tantalum pentoxide (Ta2O5) thin films for advanced dielectric applications," in Material Science and Engineering, 1998, R22, pp. 269-322.
13. A. P. E. Atanassova, "Conduction mechanisms and reliability of thermal Ta2O5–Si structures and the effect of the gate electrode," in Journal of Applied Physics, 97, 094104 s2005d, 2005, (094104), pp. 1-11.
14. J.-J. W. Fu-Chien Chiu, Joseph Ya-Min Lee, and Shich Chuan Wu, "Leakage currents in amorphous Ta2O5 thin films," in Journal of Applied Physics, 1997, 81(10), pp. 6911-6915.
15. E. Loh, "DC conduction mechanism in tantalum chip capacitors," J. Phys. D: Appl. Phys., 1980, 13, pp. 1101-1111.
16. H. W. Holland, "Solid tantalum capacitor dielectric failure mechanism and determination of failure rate," Kemet Engineering Bulletin, 1998(4).
17. B. B. F. Krahenbiihl and M. Danikas, "Properties of electrical insulating materials at cryogenic temperatures: A literature review," in EEE Electrical Insulation Magazine, 1994, 10(4), pp. 10-22.
18. J. Gill, "Surge in solid tantalum capacitors," AVX Technical Information, 1994.